Molecular Therapy
Methods & Clinical Development
Original Article

Channelrhodopsin fluorescent tag replacement for clinical translation of optogenetic hearing restoration

Maria Zerche,[1,2,3,7,9] Christian Wrobel,[2,8,9] Kathrin Kusch,[1,4] Tobias Moser,[1,5,6,7] and Thomas Mager[1,3,7]

[1]Institute for Auditory Neuroscience and InnerEarLab, University Medical Center Göttingen, 37075 Göttingen, Germany; [2]Department of Otolaryngology, University Medical Center Göttingen, 37075 Göttingen, Germany; [3]Advanced Optogenes Group, Institute for Auditory Neuroscience, University Medical Center Göttingen, 37075 Göttingen, Germany; [4]Functional Auditory Genomics, Institute for Auditory Neuroscience, University Medical Center Göttingen, 37075 Göttingen, Germany; [5]Auditory Neuroscience and Optogenetics laboratory, German Primate Center, 37077 Göttingen, Germany; [6]Auditory Neuroscience and Synaptic Nanophysiology Group, Max-Planck-Institute for Multidisciplinary Sciences, 37075 Göttingen, Germany; [7]Cluster of Excellence "Multiscale Bioimaging: from Molecular Machines to Networks of Excitable Cells" (MBExC), University of Göttingen, 37075 Göttingen, Germany; [8]Translational Inner Ear Research Group, InnerEarLab, University Medical Center Göttingen, 37075 Göttingen, Germany

Sensory restoration by optogenetic neurostimulation provides a promising future alternative to current electrical stimulation approaches. So far, channelrhodopsins (ChRs) typically contain a C-terminal fluorescent protein (FP) tag for visualization that potentially poses an additional risk for clinical translation. Previous work indicated a reduction of optogenetic stimulation efficacy upon FP removal. Here, we further optimized the fast-gating, red-light-activated ChR f-Chrimson to achieve efficient optogenetic stimulation in the absence of the C-terminal FP. Upon FP removal, we observed a massive amplitude reduction of photocurrents in transfected cells *in vitro* and of optogenetically evoked activity of the adeno-associated virus (AAV) vector-transduced auditory nerve in mice *in vivo*. Increasing the AAV vector dose restored optogenetically evoked auditory nerve activity but was confounded by neural loss. Of various C-terminal modifications, we found the replacement of the FP by the $Kir_{2.1}$ trafficking sequence ($TS_{Kir2.1}$) to best restore both photocurrents and optogenetically evoked auditory nerve activity with only mild neural loss few months after dosing. In conclusion, we consider f-Chrimson-$TS_{Kir2.1}$ to be a promising candidate for clinical translation of optogenetic neurostimulation such as by future optical cochlear implants.

INTRODUCTION

Optogenetic approaches boost research on neuronal networks and carry enormous potential for future medical treatments. In recent years, major progress has been made toward optogenetic sensory restoration. Optogenetic vision and hearing restoration combine 1D (hearing) or 2D (vision) optical stimulators and optogenetic activation of afferent neurons[1–4] via channelrhodopsins (ChRs), which are light-gated ion channels.[5,6] Vision restoration by optogenetics is currently examined in clinical trials (NCT02556736, Allergan; NCT03326336, GenSight Biologics). For hearing, to date cochlear implants (CIs) enable open-set speech recognition in a quiet background in most of the approximately 700,000 CI users. However, CI hearing is far from normal: CI users have difficulties to understand speech in multi-talker situations or the presence of background noise. This generally is assumed to result from broad spread of current from each CI electrode,[7] which limits the frequency resolution of sound coding along the tonotopic axis of the cochlea.[8] As light can be more precisely confined in space than electrical current, future optical cochlea implants (oCIs) promise sound coding with greater frequency resolution raising hope for the deaf of more natural hearing.

Optogenetic stimulation of spiral ganglion neurons (SGNs) has proven to activate the auditory pathway in various animal models of deafness.[3,4,9,10] Recently, superior spectral selectivity of optogenetic SGN stimulation in comparison with electrical CI (eCI) stimulation was demonstrated.[10–13] Aside from faithful coding of spectral information, high temporal fidelity of optogenetic stimulation is deemed important for appropriate representation of the temporal structure of acoustic stimuli and for directional hearing. Employing and engineering fast switching ChRs, such as blue-light-activated Chronos and fast (f-) and very fast (vf-) variants of the red-light-activated Chrimson[9,14–16] near-physiological firing rates of SGNs were accomplished by optogenetic stimulation. Using the fast Chrimson variants for red rather than blue light optogenetic activation minimizes the risk of phototoxicity. f-Chrimson combines fast closing kinetics

Received 22 November 2022; accepted 16 March 2023;
https://doi.org/10.1016/j.omtm.2023.03.009.

[9]These authors contributed equally

Correspondence: Christian Wrobel, Department of Otolaryngology, University Medical Center Göttingen, 37075 Göttingen, Germany.
E-mail: christian.wrobel@med.uni-goettingen.de
Correspondence: Tobias Moser, Institute for Auditory Neuroscience and InnerEarLab, University Medical Center Göttingen, 37075 Göttingen, Germany.
E-mail: tmoser@gwdg.de
Correspondence: Thomas Mager, Institute for Auditory Neuroscience and InnerEarLab, University Medical Center Göttingen, 37075 Göttingen, Germany.
E-mail: thomas.mager@med.uni-goettingen.de

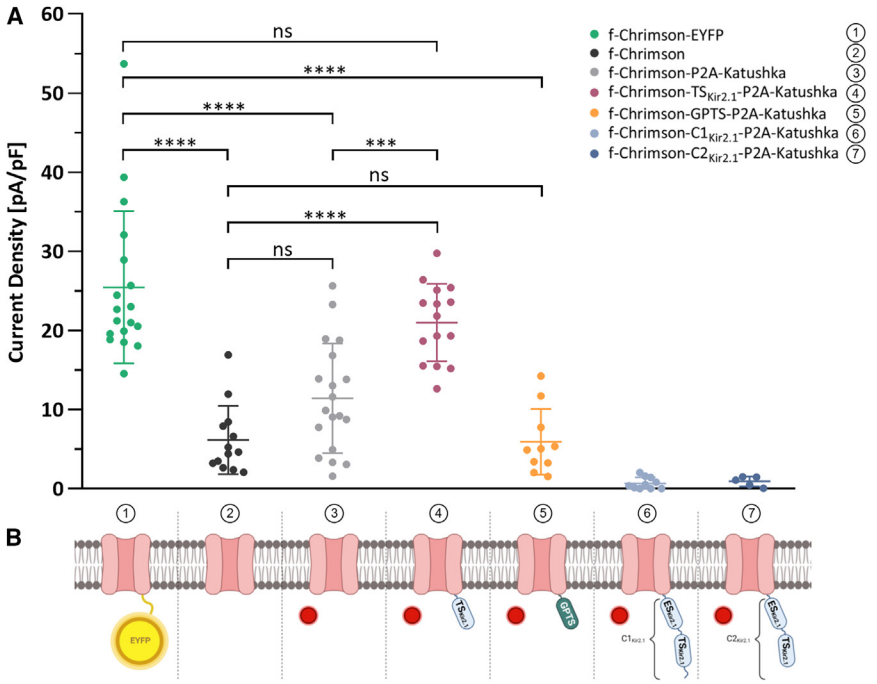

Figure 1. Effect of EYFP removal and C-terminal modifications on the photocurrent density of f-Chrimson

(A) NG cells transfected with f-Chrimson-EYFP (green, n = 18, 5 transfections), f-Chrimson* (black, n = 13, 7 transfections), f-Chrimson-P2A-Katushka (gray, n = 19, 4 transfections), f-Chrimson-TS$_{Kir2.1}$-P2A-Katushka (violet, n = 15, 5 transfections), f-Chrimson-GPTS-P2A-Katushka (orange, n = 10, 3 transfections), f-Chrimson-C1$_{Kir2.1}$-P2A-Katushka (light blue, n = 10, 3 transfections), f-Chrimson-C2$_{Kir2.1}$-P2A-Katushka (dark blue, n = 5, 2 transfections) were investigated by whole-cell patch-clamp recordings at a membrane potential of −60 mV. Photocurrents were measured upon illumination with a 500 ms light pulse of a wavelength of λ = 593 nm at saturating intensity of 21 mW/mm^2. Photocurrent densities shown were calculated as the quotient of mean stationary current and cell capacitance. Bars indicate mean and SD. Statistical analysis was performed by one-way ANOVA followed by post-hoc Bonferroni test. p values <0.05 were considered significant. Asterisks display levels of significance (****p < 0.0001, ***p < 0.001, **p < 0.01, *p < 0.05; ns, p > 0.05). (B) Graphical illustration of the modified f-Chrimson constructs. Illustrations 1–7 each refer to the construct of the photocurrent densities shown directly above in (A). In constructs 3 to 7, introduction of the self-cleaving P2A sequence, which induces ribosomal skipping during translation, leads to the separate expression of the membrane bound f-Chrimson construct and the cytosolic fluorescent signal Katushka (depicted as a red spot). The C-terminal modification of constructs 4 to 7 was achieved by adding the following sequences: (4) the Kir2.1-derived trafficking signal (TS$_{Kir2.1}$), (5) a G-protein-coupled receptor export trafficking signal (GPTS), (6) the complete export and trafficking signal of the Kir2.1 channel including a spacer sequence and the C-terminal sequence found in the Kir2.1 channel (C1$_{Kir2.1}$), (7) the export and trafficking signal of the Kir2.1 channel including a spacer sequence but without the C-terminal sequence (C2$_{Kir2.1}$).

(τ_{off} at −60 mV = 5.7 ms at room temperature) and excellent plasma membrane expression. Hence, f-Chrimson is a promising candidate for future clinical optogenetic hearing restoration. Recently, ChrimsonR, another Chrimson variant (τ_{off} at −60 mV = 15.8 ms at room temperature) has been taken to clinical trial.[2]

All previous preclinical and clinical studies on optogenetic restoration of sensory function were performed using ChRs with C-terminally fused fluorescent proteins (FPs). While allowing for a convenient detection of transfected cells in preclinical studies, the FP tag should ideally be removed for clinical trials to avoid possible adverse effects caused by the expression of an additional non-human protein. However, Gauvain et al. observed a reduced optical excitability when removing tdTomato from ChrimsonR (Chrimson K176R),[15] which was primarily attributed to a lower membrane trafficking efficacy of the untagged ChrimsonR.[17] This led to ChrimsonR-tdT being employed in a clinical optogenetic vision restoration trial.[2]

In this study, we aimed to overcome the use of a C-terminal FP tag for ChRs. We demonstrate that FP removal leads to a pronounced photocurrent decrease in f-Chrimson, which can be precluded by C-terminal fusion of the plasma membrane trafficking sequence of the human potassium channel Kir2.1 (TS$_{Kir2.1}$).[16,18,19] Utilizing adeno-associated virus (AAV)-mediated (AAV2/9) transduction of SGNs by postnatal intracochlear injections in mice, f-Chrimson-TS$_{Kir2.1}$ accordingly allowed for optically evoked auditory brainstem responses (oABRs) at low light pulse intensities and high stimulation rates. Here, with f-Chrimson-TS$_{Kir2.1}$, we present a suitable ChR for future clinical optogenetic hearing restoration.

RESULTS

Fluorescent tag removal reduces f-Chrimson photocurrents

In an attempt to further optimize f-Chrimson for clinical applications, we investigated the effect of C-terminal EYFP removal on photocurrents by whole-cell patch-clamp recordings of transfected neuroma glioblastoma (NG) cells. The electrophysiological recordings were performed 2 days after transient transfection with the respective f-Chrimson construct. The photocurrent density was measured upon illumination with a 500 ms light pulse of a wavelength of λ = 593 nm at saturating intensity (21 mW/mm^2). The mean photocurrent density in NG cells transfected with f-Chrimson-EYFP was 25.5 ± 9.6 pA/pF (n = 18; Figures 1A and 1B, illustration 1, including only fluorescent cells). Upon removal of EYFP from f-Chrimson (f-Chrimson*) the measured photocurrent density dropped significantly to 6.1 ± 4.3 pA/pF (n = 13, including only cells with measurable photocurrents). For expression control and for the assessment of the effect of a potential fluorescent cell-selection bias, additional experiments were conducted using a vector for the bicistronic expression of f-Chrimson* and the red fluorescent protein Katushka. To achieve this, we introduced the self-cleaving sequence P2A, which induces a ribosomal skipping during translation leading to the expression of two separate proteins, membrane-bound f-Chrimson* and

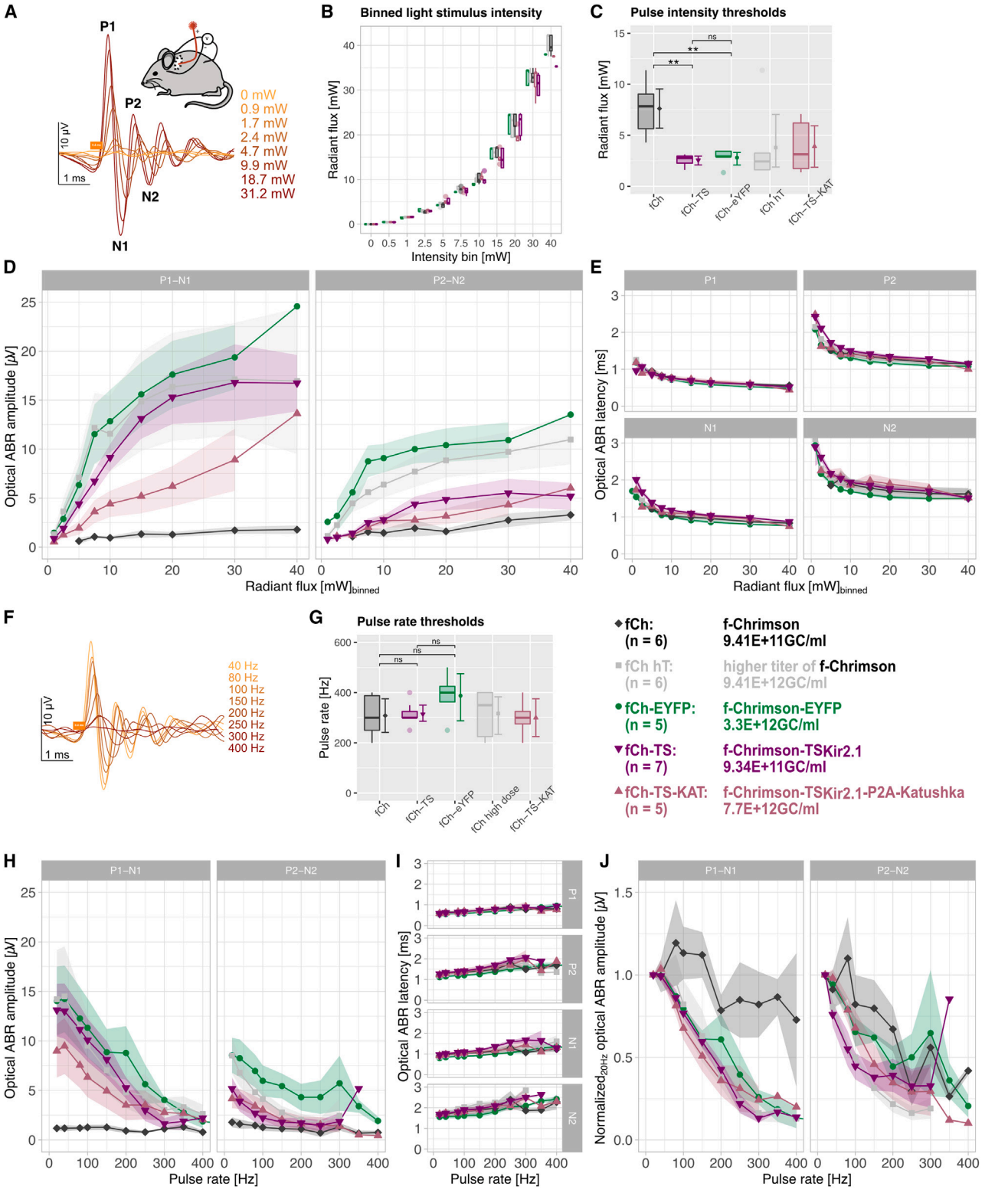

(legend on next page)

cytosolically localized Katushka (Figure 1B, illustration 3). The mean photocurrent density in f-Chrimson-P2A-Katushka transfected cells was 11.4 ± 6.9 pA/pF (n = 19), which was not significantly different to the photocurrent density measured with f-Chrimson*, but significantly smaller than the photocurrent density measured with f-Chrimson-EYFP, thereby confirming the reduction of photocurrent upon fluorescent tag removal. None of the outlined C-terminal modifications had any effect on the fast channel closing kinetics of f-Chrimson (Table S1).

Photocurrent reduction upon EYFP removal in f-Chrimson is rescued by C-terminal fusion of $TS_{Kir2.1}$

Under the assumption that the observed decrease in photocurrent upon EYFP removal is due to reduced plasma membrane expression, we tested the effect of previously described trafficking signals on the photocurrent size of f-Chrimson. In each case we used P2A-Katushka for visualizing successful transfection (Figure 1B). The C-terminal fusion of the G-protein-coupled receptor endoplasmic reticulum export trafficking sequence (GPTS)[20,21] led to a mean photocurrent density of 5.9 ± 4.1 pA/pF (n = 10, Figures 1A and 1B, illustration 5) with no significant difference to results obtained with f-Chrimson*. Improved rhodopsin targeting to the cell membranes of various cell types including SGNs has been accomplished with a construct comprising two trafficking signals ($TS_{Kir2.1}$ and $ES_{Kir2.1}$, see materials and methods) of the inward rectifying potassium channel Kir2.1 flanking a C-terminally fused EYFP.[14,16,18] Here, we tested the impact of fusing of various Kir2.1 sequences to the C terminus of f-Chrimson*: f-Chrimson-$C1_{Kir2.1}$-P2A-Katushka (Figure 1B, illustration 6), f-Chrimson-$C2_{Kir2.1}$-P2A-Katushka (Figure 1B, illustration 7), and f-Chrimson-$TS_{Kir2.1}$-P2A-Katushka (Figure 1B, illustration 4). $C1_{Kir2.1}$ contains the part of the cytosolic domain of Kir2.1 that carries both trafficking signals and the region between the trafficking signals. The addition of the C terminus of Kir2.1 to f-Chrimson-$C1_{Kir2.1}$ resulted in the construct f-Chrimson-$C2_{Kir2.1}$. In the construct f-Chrimson-$TS_{Kir2.1}$, we chose a minimal configuration in which only the trafficking sequence $TS_{Kir2.1}$ was C-terminally fused to f-Chrimson*.

The photocurrent density of f-Chrimson-$C1_{Kir2.1}$-P2A-Katushka was 0.6 ± 0.7 pA/pF (n = 10, Figure 1A) and the photocurrent density of f-Chrimson-$C2_{Kir2.1}$-P2A-Katushka was 0.92 ± 0.64 pA/pF (n = 5, Figure 1A). Hence, both constructs failed to generate sizable photocurrents. The photocurrent density measured in NG cells transfected with f-Chrimson-$TS_{Kir2.1}$-P2A-Katushka (Figure 1B, illustration 4) was 21.0 ± 4.9 pA/pF (n = 15, Figure 1A). Statistical analysis showed no significant difference between the photocurrent densities of f-Chrimson-EYFP and f-Chrimson-$TS_{Kir2.1}$-P2A-Katushka. Hence, the addition of $TS_{Kir2.1}$ to the C terminus of f-Chrimson* rescued the observed drop in photocurrent density upon fluorescent tag removal.

f-Chrimson-$TS_{Kir2.1}$ provides fast and energy-efficient optogenetic activation of the auditory pathway

Next, we compared the performance of targeting-enhanced f-Chrimson-$TS_{Kir2.1}$ with fluorescent marker-tagged f-Chrimson-EYFP as well as to f-Chrimson* employing optogenetic stimulation of the auditory nerve *in vivo*. We transduced SGNs of 6- to 7-day-old mice with the corresponding f-Chrimson constructs by injecting AAV vectors (1–1.5 μL of the according AAV2/9 suspension; AAVs and corresponding titers are listed in Figure 2) into the cochlea via the round window.[9] Subsequently, we recorded auditory brainstem responses evoked by a single-channel optical cochlear implant (oCI) in young mice 1.5–3 months after AAV injection. The basal cochlea was exposed by a retroauricular approach followed by the insertion of a 200 μm wide optical fiber into the scala tympani via the round window to deliver 594 nm laser pulses toward the basal modiolus of the cochlea (scheme in Figure 2A).

All constructs led to transduced SGNs, which upon illumination elicited oABRs with very similar waveforms but different amplitudes, quantified by the difference between the positive and negative deflections of the first as well as second oABR wave (Figure 2A, P1-N1 and P2-N2, respectively). In line with previous work using AAV2/6 as viral vector,[9] we found oABR amplitudes of mice transduced with all f-Chrimson-variants to grow (Figures 2B–2D) and oABR latencies to decline with increasing light pulse intensity (radiant flux $[mW]_{binned}$, Figure 2E). Furthermore, oABR amplitudes grew with extending light pulse durations up to 0.4 ms (Figure S2) but then decreased, likely due to decreased synchrony of SGN firing (see also Figure S3) and an emerging depolarization block of SGNs.

Figure 2. Characterizing optogenetically evoked SGN activation by auditory brainstem responses in mice upon cochlear transduction of f-Chrimson with different C-terminal modifications

(A) Exemplary optically evoked auditory brainstem responses (oABRs) at different radiant flux (1,000 repetitions of a 0.4 ms 594 nm light pulse at 20 Hz, colors code different radiant flux in mW) recorded in a mouse injected with AAV2/9-hSyn-f-Chrimson-$TS_{Kir2.1}$. oABR-waves were quantified as the difference of the positive (P1, P2) and negative (N1, N2) deflections (P1-N1, P2-N2). The insert schematizes the experimental setup for oABR recordings, with a 200 μm optical fiber placed intracochlearly via the round window. (B) Distribution of radiant flux (optical fiber output) determined prior to the recording within the different assigned bins. Different colors as well as symbols code different C-terminal modifications to f-Chrimson, consistently used across figures. (C) oABR activation thresholds by standard boxplots as well as mean ± 95% confidence intervals (point and error bars). Asterisks display levels of significance (***$p < 0.001$, **$p < 0.01$, *$p < 0.05$; ns, $p > 0.05$) in differences of C-terminal modifications (Wilcoxon rank-sum test). (D) Quantification (mean ± SEM depicted as line with points and ribbon, respectively) of oABR amplitudes by P1-N1 (left) as well as P2-N2 (right) as a function of radiant flux (binned). oABR stimulus parameters were applied as described for (A). (E) Latencies of oABR deflections (P1, P2, N1, N2) as a function of radiant flux (binned). Same dataset as in (D). (F) Exemplary oABRs of different pulse rates (1,000 repetitions of a 0.4 ms 594 nm light pulse within the 30 mW bin, colors code different pulse rates in ms) recorded in the same mouse as in (A). (G) Highest applied pulse rate (parameters correspond to F) that evoked a quantifiable oABR in terms of the detection of at least P1 and N1. Presentation and statistics correspond to (C). (H) Quantification of oABR amplitudes as a function of pulse rate, oABR stimulus parameters were applied as described for (F). (I) Latencies of oABR deflections (P1, P2, N1, N2) as a function of pulse rate. Same dataset as in (G). (J) Normalized oABR amplitudes (to 20 Hz pulse rate) as a function of pulse rate. Same dataset as in (G).

EYFP removal (f-Chrimson*) dramatically increased the oABR thresholds and reduced oABR amplitudes (Figure 2D). The threshold light intensity for f-Chrimson*—for a pulse duration of 0.4 ms and at stimulation rate of 20 Hz—of 7.6 [4.8; 10.4] mW (mean [95% confidence interval], n = 6) was significantly higher than for f-Chrimson-EYFP 2.8 [1.7; 3.9] mW (n = 5, p = 0.008, Wilcoxon rank-sum test). Adding $TS_{Kir2.1}$ to f-Chrimson* rescued the oABR thresholds (2.6 [2.0; 3.1] mW, n = 7) and P1-N1 amplitudes to the level of f-Chrimson-EYFP, which corresponded to more than one order of magnitude increase over f-Chrimson* (Figure 2D). Increasing the AAV titer by one order of magnitude (9.41E+12 GC/mL) resulted in comparable oABR results of f-Chrimson*-transduced cochleae as for f-Chrimson-$TS_{Kir2.1}$ (Figures 2B–2D). Intriguingly, f-Chrimson-$TS_{Kir2.1}$-P2A-Katushka, despite administration at a higher AAV titer (7.7E+12 GC/mL) than f-Chrimson-$TS_{Kir2.1}$ did not achieve oABR amplitude levels of f-Chrimson-$TS_{Kir2.1}$ (Figure 2D). The lowest possible energy per light pulse—0.04 ms duration presented at 20 Hz—sufficient to evoke an oABR in f-Chrimson-$TS_{Kir2.1}$-transduced mice amounted to 0.3 [0.1; 0.5] μJ (Figure S3).

Optically evoked ABRs remained measurable at least up to stimulation rates of 300 Hz—presented at 0.4 ms light pulse duration with radiant flux in the 30 mW bin—and even higher in individual animals (Figures 2F–2H). oABR latencies increased upon raising stimulation rate across mice transduced with the different f-Chrimson variants (Figure 2I). The lack of an obvious stimulation-rate modulation of oABR amplitude and latency in mice transduced with f-Chrimson* might have resulted from a suboptimal signal to noise ratio due to lower ChR abundance in the SGN-membrane (Figure 2J).

Favorable cochlear safety profile of AAV2/9-hSyn-f-Chrimson-$TS_{Kir2.1}$

Here, we thoroughly assessed SGN-density in mice at 1.5–3 months of age following postnatal AAV-injection for the different C-terminally modified f-Chrimson variants in immunolabeled cochlear cryosections (Figure 3A). Since there is currently no antibody available to directly label f-Chrimson for immunofluorescent analysis, the fraction of SGNs transduced with un-labeled f-Chrimson variants was estimated by the co-expressed EYFP or Katushka (P2A cleavage).

As controls we analyzed both ears of non-injected wild-type (WT) mice that showed no significant differences of SGN cell density between ears or different cochlear turns (p > 0.05, Wilcoxon rank-sum test, Figure 3B). Cochleae injected with AAV2/9-hSyn-f-Chrimson* (9.4×10^{11} GC/mL) showed very similar SGN cell density (Figure 3B), while at the higher titer (9.4×10^{12} GC/mL) substantial SGN loss of 34% was found on the injected side (p = 0.003, Wilcoxon rank-sum test). The analysis of SGN density in the other f-Chrimson variants suggested a mild SGN loss with an apical to basal cochlear gradient (Figures 3B and 3C). The fraction of transduced SGNs in cochleae treated with f-Chrimson-EYFP and f-Chrimson-$TS_{Kir2.1}$-P2A-Katushka revealed an apical to basal cochlear gradient of SGN transduction (Figure S4B), suggesting a causal effect of transgene expression on SGN integrity as postulated in a prior study.[22] The integrity and presence of contaminating proteins from AAV vector production was controlled by electron microscopy and SDS-PAGE, respectively, of all vector preparations used (Figure S5). Of note, integrity and purity were comparable for f-Chrimson, f-Chrimson-EYFP. and f-Chrimson-TS $_{Kir2.1}$-P2A-Katushka, but detectably lower for f-Chrimson-$TS_{Kir2.1}$. Therefore, we conclude that the toxic effects postulated for f-Chrimson* are unlikely due to contaminants or immunogenic empty AAV particles. We note that, as described previously,[14,16] transduction was also observed in the non-injected (right) ear, likely due to spread of AAV via cochlear aqueducts and the cerebrospinal fluid space (Figure S4B), which could explain the lack of SGN density differences between both ears in some animals. Rescue of oABR amplitudes utilizing f-Chrimson-$TS_{Kir2.1}$ implied moderate SGN decrease only in the apical cochlear turn in comparison with non-injected mice (p = 0.026, Wilcoxon rank-sum test, Figure 3C). Referring to comparable oABR results, SGN loss was determined for f-Chrimson-EYFP as well as for a high titer of AAVs delivering f-Chrimson* in the apical cochlear turn (p = 0.03 and p = 0.009, respectively, Wilcoxon rank-sum test), plus furthermore profoundly in the middle cochlear turn (p = 0.004 and p = 0.002, respectively, Wilcoxon rank-sum test; Figure 3C) in comparison with non-injected mice.

DISCUSSION

Since the discovery of ChRs, C-terminally truncated constructs, essentially comprising the 7-transmembrane helix (TMH) motif, have been employed in optogenetics, mainly because (1) the C-terminal truncation of the cytoplasmic domain did not impair channel function in ChR1 and ChR2[5,6] and (2) cargo capacity of vectors for gene transfer is limited. Accordingly, metagenomic screenings for advanced ChRs and their subsequent functional characterizations were conducted with protein sequences, which only comprise the TMH motif.[15,23] Frequently, those shortened optogenes are C-terminally fused to a fluorescent marker protein, which enables the convenient assessment of their expression and subcellular localization. Recently, preclinical work on non-human primate retinal explants[17] showed that the probability of obtaining light-evoked responses of retinal ganglion cells was considerably lower upon FP removal from the C terminus of ChrimsonR.

The pronounced photocurrent decrease upon EYFP removal that we observed in NG cells, and our finding that it can be precluded by the C-terminal fusion of $TS_{Kir2.1}$, indicates that fluorescent tag removal likely affects plasma membrane expression of f-Chrimson (Chrimson Y261F/S267M). Furthermore, we provide a possible explanation for the results obtained in non-human primates, which led to ChrimsonR, C-terminally fused to tdT, being employed for a clinical study on optogenetic vision restoration.[2] En route to clinical translation, we deem the C-terminal replacement of tdT against the trafficking sequence of the human potassium channel $Kir_{2.1}$ ($TS_{Kir2.1}$) important, because the gene therapeutic use of an additional non-human protein is not justified if it is not essential for the treatment and because co-expression of FP may lead to a stronger immune reaction in the patient. Moreover, the packing capacity of AAV variants, which are

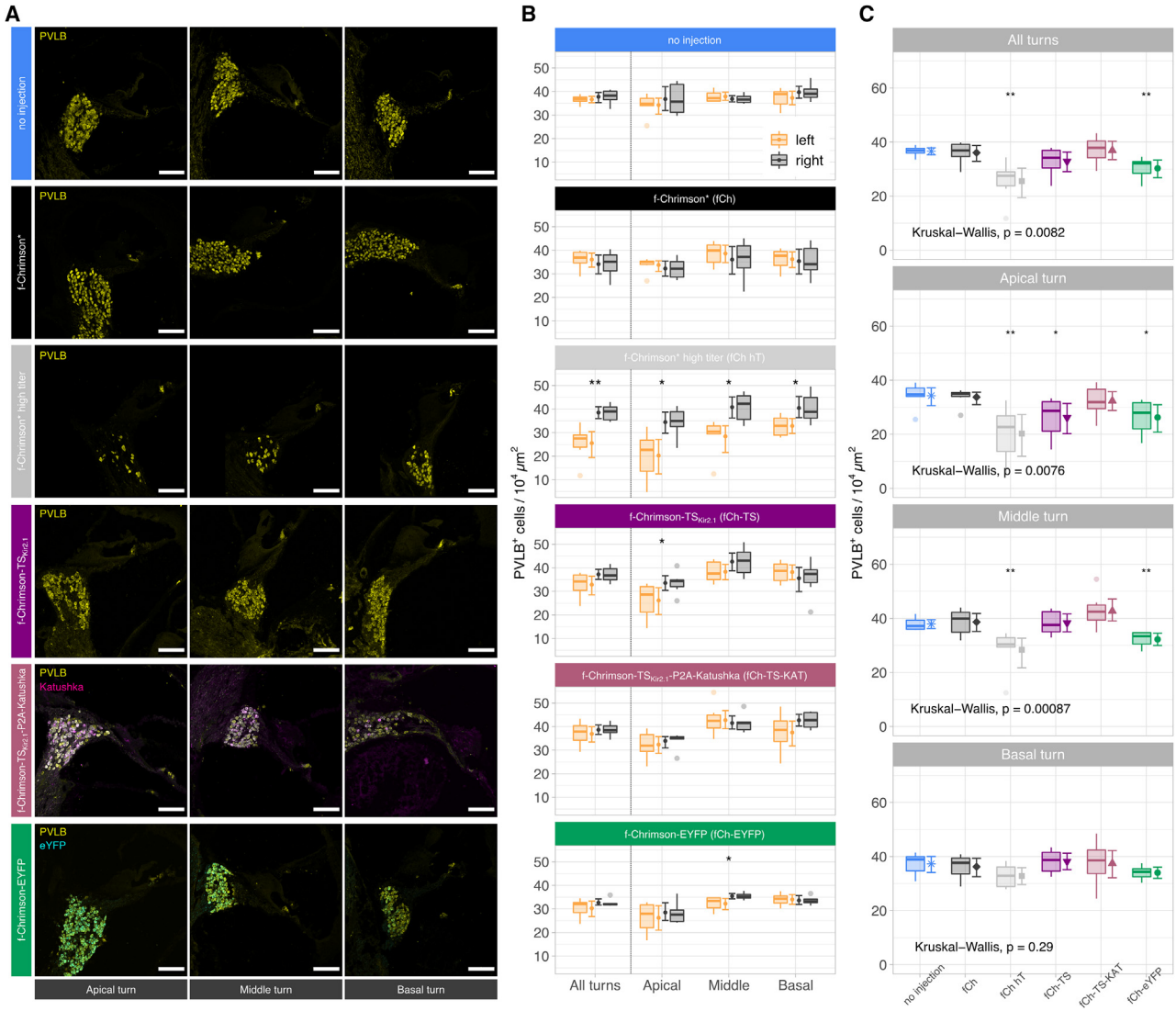

Figure 3. Quantification of neuron density in the spiral ganglion

(A) Maximum projection of immunolabeled (PVLB [parvalbumin], yellow; Katushka, magenta; EYFP [enhanced yellow fluorescent protein], green) confocal images of the apical, middle, and basal spiral ganglion of the left AAV-injected side. Presentation of exemplary mid-modiolar cryosections of mice cochlea transduced with f-Chrimson with different C-terminal modifications. Scale bar, 100 µm. (B) Density of spiral ganglion neurons (SGNs) comparing the left f-Chrimson injected side with the uninjected right cochlea. Total SGN density of the apical, middle, and basal cochlear turn is depicted by standard boxplots as well as mean ± 95% confidence interval (point and error bars). Asterisks display levels of significance (***p < 0.001, **p < 0.01, *p < 0.05; ns, p > 0.05) in differences of sides (Wilcoxon rank-sum test). (C) SGN density comparing f-Chrimson-groups of different C-terminal modification (left AAV-injected side) presented for the apical, middle, and basal spiral ganglion as well as in summation (total). Kruskal-Wallis statistics was employed to detect differences between groups, asterisks display different levels of significance (Wilcoxon rank-sum test). Presentation corresponds to (B).

used in human gene therapy, is limited to ~4.8 kb. Replacing EYFP (717 bp) against $TS_{Kir2.1}$ (60 bp) extends free packing capacity in the AAV vectors. The increase of free packing capacity will allow the use of larger promotors, which may combine higher cell type specificity with balanced expression strength in the future. As explained in detail in the following, we consider f-Chrimson-$TS_{Kir2.1}$ a suitable optogene for use in the future oCI.

Stimulation of the auditory system by future optical CIs requires appropriate SGN activation at high pace in conjunction with high energy efficiency. The targets are the physiological sound-evoked SGN firing rate of hundreds of Hertz and the temporal fidelity in the sub-millisecond range.[24] Recordings of far-field neural population responses of the auditory brainstem upon optical stimulation of f-Chrimson-$TS_{Kir2.1}$-transduced SGNs in mice revealed

energy thresholds of 0.3 μJ on average. This is close to typical pulse energies used for electrical stimulation (0.2 μJ for biphasic pulses of 80 μs,[25]) and in line with our previous estimate of ∼0.5 μJ for AAV2/6-hSyn-f-Chrimson-EYFP in mice,[9] while higher thresholds of 1–2 μJ were found for AAV2/6-hSyn-CatCh-EYFP in gerbils[3] and 6–14 μJ for PHP.B-hSyn-Chronos-$TS_{Kir2.1}$-EYFP-$ES_{Kir2.1}$ or -Chronos-EGFP.[16,26] This suggests feasible energy budgets for f-Chrimson-$TS_{Kir2.1}$-mediated clinical hearing restoration, where (1) more efficient emitter placement will be used (along scala tympani rather than emitter placement at the round window used here) and (2) upscaling the number of channels (from currently 12–24 in eCI to 64 in oCI) will be partially offset by lower pulse rates per channels (e.g., 200 Hz in oCI compared with ∼900 Hz in eCIs) expected to drive near-physiological rates and synchrony of firing.

Indeed, the temporal fidelity of AAV2/9-hSyn-f-Chrimson-$TS_{Kir2.1}$-mediated auditory nerve stimulation—at least 300 Hz, estimated on a neural population level—was comparable with that of f-Chrimson-EYFP for which furthermore recordings from single SGNs substantial phase locking to light pulses (vector strength $\geq$50% was found up to stimulation rates of ∼250 Hz (AAV2/6-hSyn-f-Chrimson-EYFP[9]). Achieving even higher temporal fidelity of optical coding in the auditory system currently comes at the expense of elevated energy thresholds, as shown for Chronos with even shorter-lived open states than f-Chrimson (τ_{off}: 0.8 ms at physiological temperature[16] vs. 3.2 ms f-Chrimson[9]).

In view of the clinical application of optical CIs, size as well as xenogeny of the transduced protein should optimally be as low as possible. The most obvious approach was EYFP removal (f-Chrimson*), which, however, resulted in a drastic decrease of oABR amplitudes of more than one order of magnitude as well as a significant increase in energy thresholds to evoke auditory responses. Fusing an FP to ChRs can modulate their functional properties: e.g., neurons expressing ChR2 fused to EYFP provided higher photosensitivity to neurons than ChR2 fused to tdTomato in a similar transgenic approach.[27] Multiple intracellular processes such as ER exiting, protein folding as well as membrane trafficking are conceivable reasons. Gauvain et al. observed distinct optical excitability between ChrimsonR fused to tdTomato and its naive variant, which was primarily attributed to a lower membrane trafficking efficacy of untagged ChrimsonR.[17] Here, we could substantiate this assumption by C-terminal fusion of the plasma membrane trafficking sequence of the human potassium channel Kir2.1 to f-Chrimson,[16,18,19] which rescued fast and energy efficient optogenetic activation of the auditory system to the levels observed with the EYFP-fused variant of f-Chrimson.

Future clinical application of f-Chrimson as a suitable candidate for hearing restoration by optical CIs rests on the lack of adverse effects like SGN loss due to neural degeneration induced by protein toxicity and/or immune responses. Mice transduced with f-Chrimson-EYFP as well as mice injected with a high titer of AAV2/9 carrying f-Chrimson*, providing ABR results comparable with those with f-Chrimson-$TS_{Kir2.1}$, showed a substantial decrease in SGN density in comparison with WT cochleae, which was not seen for f-Chrimson-$TS_{Kir2.1}$. Together, our results suggest that AAV dose- and protein-dependent effects can lead to SGN loss. Accurate protein folding and membrane trafficking are complex but crucial, especially in the context of microbial opsin expression in eukaryotic cells.[28] Impairment of these processes—by aggregation in the endoplasmatic reticulum, trafficking defects, and/or formation of aggregates—could potentially induce cell stress of a toxic level. Heavy overexpression of the optogenetic actuator, e.g., in the case of the administration of too high AAV titers of AAV2/9-hSyn-f-Chrimson*, may therefore result in cell-damaging stress. In the case of f-Chrimson-EYFP, overexpression of the fluorescent reporter may have contributed to increased SGN loss, which has been reported in several studies including evidence of neurotoxicity.[29,30] We assume that the previously observed lack of significant SGN loss at 1 and 3 months of AAV2/6-mediated f-Chrimson-EYFP expression might reflect the low sample size in the prior study or the use of different AAVs.[22] Contributions of immune responses to AAV2/9 dosing are unlikely as the AAV dose that efficiently transduced f-Chrimson-$TS_{Kir2.1}$ into SGNs had no impact on SGN density when transducing f-Chrimson*. Moreover, in their longitudinal study on stability and safety of postnatal AAV2/6-hSyn-f-Chrimson-EYFP dosing in mice,[22] Bali et al. also described an apicobasal gradient of age-related SGN loss but did not notice signs of inflammation or leukocyte infiltration in HE stainings at any point in time. Together, the present and previous data indicate stable f-Chrimson expression in rodent SGNs over months without obvious immune responses and with mild SGN loss beyond their naturally occurring age-related diminution.[9,14,22] In fact, the present data (1.5–3 months after injection) suggest better SGN survival with transduction of f-Chrimson-$TS_{Kir2.1}$ compared with the EYFP-tagged variant employed in the latter studies. Evidence of immunological reactions to microbial opsin-transduced peripheral mammal neurons has been reported.[31] Therefore, careful preclinical analysis of potential innate and adaptive cochlear immune responses to AAV vector dosing and ChR expression in the cochlea and, if present, their pharmacological control, remains an important objective en route to clinical translation.

Together, this study indicates that f-Chrimson-$TS_{Kir2.1}$ is a promising candidate for optogenetic hearing restoration. Combining good membrane targeting, red-shifted action spectrum and fast-closing kinetics, f-Chrimson-$TS_{Kir2.1}$ enables light-controlled SGN spiking at near physiological rates with relatively low light requirements and risk of phototoxicity. Herewith, we demonstrate a feasible way to avoid the expression of an additional non-human protein with potential adverse effects in the human ear, which we consider an important step toward a clinical application in the future oCI.

MATERIALS AND METHODS

Molecular biology

f-Chrimson-$C1_{Kir2.1}$, f-Chrimson-$C2_{Kir2.1}$, f-Chrimson-$TS_{Kir2.1}$, and f-Chrimson-GPTS, were produced by PCR-based cloning using the human codon optimized sequence of f-Chrimson[9] and the synthesized DNA sequence coding for the α2B-adrenergic receptor trafficking

sequence GPTS (FNQDFRRAFRRILCRPWTQTGW) or the DNA sequences coding for $C1_{Kir2.1}$ (LVFSHNAVIAMRDGKLCLMWRVG NLRKSHL–VEAHVRAQLLKSRITSEGEYIPLDQIDINVGFDSGIDR IFLVSPITIVHEIDEDSPLYDLSKQDIDNADFEIVVILEGMVEATA MTTQCRSSYLANEILWGHRYEPVLFEEKHYYKVDYSRFHKTYE VPNTPLCSARDLAEKKYILSNANSFCYENEVA) and $C2_{Kir2.1}$ (LVF SHN-AVIAMRDGKLCLMWRVGNLRKSHLVEAHVRAQLLKSRIT SEGEYIPLDQIDINVGFDSGIDRIFLVSPITIVHEIDEDSPLYDLSKQ DIDNADFEIVVILEGMVEATAMTTQCRSSYLANEILWGHRYEPV LFEEKHYYKVDYSRFHKTYEVPNTPLCSARDLAEKKYILSNANSF CYENEVALTSKEEDDSENGVPESTSTDTPPDIDLHNQASVPLEPR PLRRESEI), which were derived from human Kir2.1 (plasmid no. 107184, Addgene). $C1_{Kir2.1}$ and $C2_{Kir2.1}$ include the trafficking sequence $TS_{Kir2.1}$ (KSRITSEGEYIPLDQIDINV) and the ER export sequence $ES_{Kir2.1}$ (FCYENEV). Chrimson-$C1_{Kir2.1}$, f-Chrimson-$C2_{Kir2.1}$, and f-Chrimson-GPTS were cloned into a pcDNA3.1 derivative (Invitrogen, Carlsbad, CA, and Shevchenko et al.[19]), 5′ to the DNA sequences coding for the self-cleaving sequence P2A and the red fluorescent protein Katushka. f-Chrimson was cloned into the same pcDNA3.1 derivative (Invitrogen and Shevchenko et al.[19]) 5′ to DNA sequences coding for $TS_{Kir2.1}$, the self-cleaving sequence P2A, and the red fluorescent protein Katushka. f-Chrimson-$TS_{Kir2.1}$ and f-Chrimson-$TS_{Kir2.1}$-P2A-Katushka were subcloned into a pAAV2 vector[32] carrying the human synapsin promoter, the woodchuck hepatitis virus posttranscriptional regulatory element and a polyadenylation site derived SV40.

AAV vector production

AAV vectors were generated in HEK293T cells (ATCC) using polyethylenimine transfection (Polysciences). The cell line was tested negatively for mycoplasma. In brief, triple transfection of HEK293T cells was performed using the pHelper plasmid (TaKaRa/Clontech), the *trans*-plasmid providing viral capsid AAV2/9 and the *cis*-plasmid providing f-Chrimson-$TS_{Kir2.1}$, f-Chrimson-$TS_{Kir2.1}$-P2A-Katushka, f-Chrimson-EYFP, or f-Chrimson, respectively. The viral particles were harvested 72 h after transfection from the medium and 120 h after transfection from cells and the medium. Viral particles from the medium were precipitated with 8% polyethylene glycol 8000 (Acros Organics, Germany) in 500 mM NaCl for 2 h at 4°C and, after centrifugation at 4,000 × *g* for 30 min, resuspended in 500 mM NaCl, 40 mM Tris, 2.5 mM $MgCl_2$ (pH 8), and 100 U/mL of salt-activated nuclease (Arcticzymes) and incubated at 37°C for 30 min. Similarly, cell pellets were suspended in 500 mM NaCl, 40 mM Tris, 2.5 mM $MgCl_2$ (pH 8), and 100 U/mL of salt-activated nuclease (Arcticzymes) at 37°C for 90 min. After pooling both fractions, the lysates were cleared at 2,000 × *g* for 10 min and AAV vectors were purified over iodixanol (OptiPrep, Axis Shield, Norway) step gradients (15%, 25%, 40%, and 60% at 351,000 × *g* for 2.25 h. AAV vectors were concentrated using Amicon filters (EMD, UFC910024) and formulated in sterile phosphate-buffered saline supplemented with 0.001% Pluronic F-68 (Gibco, Germany). AAV vector titers were measured using an AAV titration kit (TaKaRa/Clontech) according to the manufacturer's instructions by determining the number of DNase I-resistant vector genomes using qPCR (StepOne, Applied Biosystems). Purity of produced vectors was routinely checked by silver staining (Pierce, Germany) after gel electrophoresis (Novex 4–12% Tris-Glycine, Thermo Fisher Scientific) according to manufacturer's instruction. The presence of viral capsid proteins was positively confirmed in all AAV vector preparations by electron microscopy upon negative staining of AAV vectors that adhered to plasma-treated carbon support film 200 mesh grids (Electron Microscopy Sciences) and the percentage of filled capsids was calculated from all AAV vector profiles on five to eight randomly chosen fields of view at magnification of 20,000× on a Jem-1011 (Jeol).

Cell culture and transfection

For *in vitro* analysis of f-Chrimson variants, the NG cell line NG108-15 was used. NG108-15 cells (ATCC, HB-12377TM, Manassas, VA) were cultured in Dulbecco's modified Eagle medium (DMEM) (Sigma, St. Louis, MO) supplemented with 10% fetal calf serum (Sigma) and 5% penicillin/streptomycin (Sigma) at 37°C and 5% CO_2. Cells were seeded on 24-well plates 1 day before transfection and were transfected at a confluency of 70%–80%. Transfection with pcDNA3.1(−) carrying the described f-Chrimson constructs was achieved via Lipofectamine transfection. For each well a transfection mix of 100 µL DMEM and 3 µL Lipofectamine LTX (Invitrogen) and 500 ng of plasmid pcDNA3.1(−) was prepared and added to a well with 400 µL of DMEM. Twenty-four hours after transfection the medium was changed and supplemented with 1 µmol retinal.

Electrophysiological recordings

Electrophysiological characterization of f-Chrimson variants was performed by whole-cell patch-clamp recordings of NG108-15 cells expressing the respective ChR variant (see Figure S1A). Cells were patched 2 days after transfection under voltage clamp conditions using an Axopatch 200B amplifier (Axon Instruments, Union City, CA) and a DigiData 1322A interface (Axon Instruments). Patch pipettes with a resistance of 2–6 MΩ were fabricated from thin-walled borosilicate glass on a horizontal puller (Model P-1000, Sutter Instruments, Novato, CA). The series resistance was <15 MΩ. The bath solution contained 140 mM NaCl, 2 mM $CaCl_2$, 2 mM $MgCl_2$, and 10 mM HEPES (pH 7.4), and the pipette solution contained 110 mM NaCl, 2 mM $MgCl_2$, 10 mM EGTA, and 10 mM HEPES (pH 7.4). All recordings were performed at room temperature (297 K). For determination and comparison of current densities and off-kinetics, NG108-15 cells heterologously expressing the aforementioned f-Chrimson variants were investigated at a membrane potential of −60 mV. Photocurrents were measured in response to 500 or 3 ms light pulses with a saturating intensity of 21 mW/mm^2 using a diode-pumped solid-state laser (λ = 593) focused into a 400 µm optic fiber. Light pulses were applied by a fast computer-controlled shutter (Uniblitz LS6ZM2, Vincent Associates, Rochester, NY). Current densities (J-60 mV) were calculated as the quotient of the stationary current measured in response to a 500 ms light pulse with a saturating intensity of 21 mW/mm^2 and the capacitance of the cell. τ_{off} values were determined by a fit of a monoexponential function to the decaying photocurrent elicited in response to a 3 ms light pulse. To reduce experimental bias, cells expressing constructs containing EYFP or

Katushka were chosen for the electrophysiological recordings independent of the brightness of their fluorescent signal.

Postnatal intracochlear AAV injections

The left cochlea of C57BL/6 WT mice (p6-p7) was injected with AAV2/9 suspensions via the round window to transduce SGNs with different f-Chrimson variants. The neural specificity of the transgenic expression was obtained by employing the human synapsin-1 gene promoter. As described previously,[9,16,33] animals were anesthetized using isoflurane inhalation and xylocaine was applied retro-auricularly for local analgesia. A retro-auricular incision of the skin was performed and subsequently the cartilaginous bulla exposed. After identification of the basal cochlea, approximately 1–1.5 μL of the AAV vector suspension was injected into the scala tympani utilizing a borosilicate capillary pipette by gently puncturing the round window membrane. The different administered titers of the AAV vector suspension (volumes were kept constant by diluting suspensions to the required titers) are listed in Figure 2. The bulla was sealed by repositioning of the overlaying tissue and the wound was sutured. Post-surgery, buprenorphine (0.1 mg kg^{-1}) and carprofen (5 mg kg^{-1}) were applied for pain relief and the animals were tracked daily. Animals were then kept in a 12 h light/dark cycle with access to food and water *ad libitum*. All experiments were done in compliance with the national animal care guidelines and were approved by the board for animal welfare of the University Medical Center Göttingen and the animal welfare office of the state of Lower Saxony (LAVES; 17/2394).

oABR recordings

Animals, age 1.5–3 months, were anesthetized by isoflurane inhalation, and buprenorphine (0.1 mg kg^{-1}) as well as carprofen (5 mg kg^{-1}) were applied by subcutaneous injections as analgesics. The mice were placed on a custom-built heating plate (at 38°C) on a vibration isolation table within a soundproof chamber (Industrial Acoustics). The round window of the left injected cochlea was surgically approached retro-auricularly by incision of the skin, exposing and partially opening the bulla. A 200 μm optical fiber coupled to a 594 nm laser (OBIS LS OPSL, 100 mW, Coherent) was inserted via the round window and oriented toward the basal modiolus. Needle electrodes were inserted underneath the pinna, on the vertex, and on the back near the tail of the animal.

Generation and presentation of optical stimuli as well as data acquisition were realized by custom-written MATLAB software (The MathWorks) employing National Instruments data acquisition (NI-DAQ) cards in combination with custom-built hardware to control laser drivers and to acquire data. Irradiance was calibrated for every experiment with a laser power meter (LaserCheck; Coherent). The potential difference between subdermal needles of the vertex and the mastoid was amplified using a custom-designed amplifier, sampled at a rate of 50 kHz (NI PCI-6229, National Instruments), and filtered offline (300–3,000 Hz Butterworth filter). oABR thresholds as well as deflections (P1, N1, P2, N2) were determined semi-automatically by custom code (Python Software Foundation, Python Language Reference, version 3.9.1) and subsequent visual inspection.

Cochlear cryosections, immunolabeling, and imaging

The cochleae of both sides were extracted from the temporal bone immediately after finishing the ABR experiment and fixed in 4% paraformaldehyde in phosphate buffer for 40 min at 4°C. For cryosectioning, cochleae were decalcified in ethylenediaminetetraacetic acid (0.12 M for 3–5 days). Immunolabeling was performed on 16 μm thin mid-modiolar cryosections utilizing goat serum dilution buffer (16% normal goat serum, 450 mM NaCl, 0.6% Triton X-100, and 20 mM phosphate buffer [pH 7.4]). The following primary antibodies were applied: guinea pig anti-parvalbumin (catalog no. 195004, Synaptic Systems, 1:300), rabbit Alexa Fluor 488-conjugated GFP (catalog no. A-21311, Thermo Fisher Scientific, 1:300), rabbit anti-turboRFP (catalog no. AB233, evrogen, 1:300). The following Alexa Fluor-labeled secondary antibodies were applied, respectively: goat anti-guinea pig 647 IgG-H+L (catalog no. A1107, Thermo Fisher Scientific, 1:200), goat anti-rabbit 568 IgG-H+L (catalog no. A11011, Thermo Fisher Scientific, 1:200).

Confocal images were acquired using a Leica-SP8 microscope (Leica, Hamburg, Germany) and processed in ImageJ (NIH, Bethesda, MD). Expression was considered positive when EYFP- or Katushka-labeled fluorescence in a given cell (marked by parvalbumin) was found to be higher than 3 SD above the background fluorescence of the tissue.

Data analysis

The open-source statistic software "R" (packages: Hmisc, ggplot2, ggpubr, dplyr) as well as Origin 9.0 (OriginLab, Northampton, MA) and GraphPad Prism (GraphPad Software, La Jolla, CA) were employed for statistical and graphical data analysis. Averages are expressed as mean ± 95% confidence interval or mean ± standard error of the mean, where most appropriate. Statistical analysis of normally distributed data was performed by one-way ANOVA followed by post-hoc Bonferroni test. Since ABR data was not normally distributed (Shapiro-Wilk test), the Wilcoxon rank-sum test (two sided; paired or unpaired where applicable) was utilized to compare the two groups. For the comparison of multiple groups, the Kruskal-Wallis test (unpaired, two sided) followed by a pairwise Wilcoxon test (post-hoc analysis, Bonferroni-adjustment of p value) were performed. Alpha levels were set at 0.05 (*), 0.01 (**), 0.001 (***), and 0.0001 (****).

DATA AVAILABILITY

The data that support the findings of this study and code used for analysis are available from the corresponding authors upon reasonable request.

SUPPLEMENTAL INFORMATION

Supplemental information can be found online at https://doi.org/10.1016/j.omtm.2023.03.009.

ACKNOWLEDGMENTS

We thank Christiane Senger-Freitag for expert help with cloning of the f-Chrimson constructs and excellent technical support. We

thank Daniela Gerke for expert help with AAV vector and immunolabeled mid-modiolar cochlear cryosection preparation and Sandra Gerke for expert technical support, Gerhard Hoch for his expert engineering support, Lena Lindner for performing histology, and Patricia Raeke-Kuegler for excellent administrative support. This work was funded by the Fraunhofer and Max-Planck cooperation program (NeurOpto grant) to T.M. and was further supported by the German Research Foundation through the Cluster of Excellence (EXC2067) Multiscale Bioimaging to T. Mager, M.Z., and T. Moser as well as the Leibniz Program to T. Moser. In addition, this research is supported by Fondation Pour l'Audition (FPA RD-2020-10) to T. Moser.

AUTHOR CONTRIBUTIONS

C.W., T. Mager, and T. Moser designed research. T. Mager cloned the f-Chrimson constructs and supervised the patch-clamp experiments. M.Z. performed the patch-clamp experiments and analyzed data. C.W. performed oABR measurements, immunohistochemistry and analyzed data. K.K. prepared the AAVs. M.Z., C.W., T. Moser, and T. Mager wrote the manuscript.

DECLARATION OF INTERESTS

The authors declare no competing interests.

REFERENCES

1. Bi, A., Cui, J., Ma, Y.P., Olshevskaya, E., Pu, M., Dizhoor, A.M., and Pan, Z.H. (2006). Ectopic expression of a microbial-type rhodopsin restores visual responses in mice with photoreceptor degeneration. Neuron *50*, 23–33.
2. Sahel, J.A., Boulanger-Scemama, E., Pagot, C., Arleo, A., Galluppi, F., Martel, J.N., Esposti, S.D., Delaux, A., de Saint Aubert, J.B., de Montleau, C., et al. (2021). Partial recovery of visual function in a blind patient after optogenetic therapy. Nat. Med. *27*, 1223–1229.
3. Wrobel, C., Dieter, A., Huet, A., Keppeler, D., Duque-Afonso, C.J., Vogl, C., Hoch, G., Jeschke, M., and Moser, T. (2018). Optogenetic stimulation of cochlear neurons activates the auditory pathway and restores auditory-driven behavior in deaf adult gerbils. Sci. Transl. Med. *10*, eaao0540.
4. Hernandez, V.H., Gehrt, A., Reuter, K., Jing, Z., Jeschke, M., Mendoza Schulz, A., Hoch, G., Bartels, M., Vogt, G., Garnham, C.W., et al. (2014). Optogenetic stimulation of the auditory pathway. J. Clin. Invest. *124*, 1114–1129.
5. Nagel, G., Ollig, D., Fuhrmann, M., Kateriya, S., Musti, A.M., Bamberg, E., and Hegemann, P. (2002). Channelrhodopsin-1: a light-gated proton channel in green algae. Science *296*, 2395–2398.
6. Nagel, G., Szellas, T., Huhn, W., Kateriya, S., Adeishvili, N., Berthold, P., Ollig, D., Hegemann, P., and Bamberg, E. (2003). Channelrhodopsin-2, a directly light-gated cation-selective membrane channel. Proc. Natl. Acad. Sci. USA *100*, 13940–13945.
7. Kral, A., Hartmann, R., Mortazavi, D., and Klinke, R. (1998). Spatial resolution of cochlear implants: the electrical field and excitation of auditory afferents. Hear. Res. *121*, 11–28.
8. Friesen, L.M., Shannon, R.V., Baskent, D., and Wang, X. (2001). Speech recognition in noise as a function of the number of spectral channels: comparison of acoustic hearing and cochlear implants. J. Acoust. Soc. Am. *110*, 1150–1163.
9. Mager, T., Lopez de la Morena, D., Senn, V., Schlotte, J., D Errico, A., Feldbauer, K., Wrobel, C., Jung, S., Bodensiek, K., Rankovic, V., et al. (2018). High frequency neural spiking and auditory signaling by ultrafast red-shifted optogenetics. Nat. Commun. *9*, 1750.
10. Keppeler, D., Schwaerzle, M., Harczos, T., Jablonski, L., Dieter, A., Wolf, B., Ayub, S., Vogl, C., Wrobel, C., Hoch, G., et al. (2020). Multichannel optogenetic stimulation of the auditory pathway using microfabricated LED cochlear implants in rodents. Sci. Transl. Med. *12*, eabb8086.
11. Dieter, A., Duque-Afonso, C.J., Rankovic, V., Jeschke, M., and Moser, T. (2019). Near physiological spectral selectivity of cochlear optogenetics. Nat. Commun. *10*, 1962.
12. Dieter, A., Klein, E., Keppeler, D., Jablonski, L., Harczos, T., Hoch, G., Rankovic, V., Paul, O., Jeschke, M., Ruther, P., and Moser, T. (2020). muLED-based optical cochlear implants for spectrally selective activation of the auditory nerve. EMBO Mol. Med. *12*, e12387.
13. Khurana, L., Keppeler, D., Jablonski, L., and Moser, T. (2022). Model-based prediction of optogenetic sound encoding in the human cochlea by future optical cochlear implants. Comput. Struct. Biotechnol. J. *20*, 3621–3629.
14. Bali, B., Lopez de la Morena, D., Mittring, A., Mager, T., Rankovic, V., Huet, A.T., and Moser, T. (2021). Utility of red-light ultrafast optogenetic stimulation of the auditory pathway. EMBO Mol. Med. *13*, e13391.
15. Klapoetke, N.C., Murata, Y., Kim, S.S., Pulver, S.R., Birdsey-Benson, A., Cho, Y.K., Morimoto, T.K., Chuong, A.S., Carpenter, E.J., Tian, Z., et al. (2014). Independent optical excitation of distinct neural populations. Nat. Methods *11*, 338–346.
16. Keppeler, D., Merino, R.M., Lopez de la Morena, D., Bali, B., Huet, A.T., Gehrt, A., Wrobel, C., Subramanian, S., Dombrowski, T., Wolf, F., et al. (2018). Ultrafast optogenetic stimulation of the auditory pathway by targeting-optimized Chronos. EMBO J. *37*, e99649.
17. Gauvain, G., Akolkar, H., Chaffiol, A., Arcizet, F., Khoei, M.A., Desrosiers, M., Jaillard, C., Caplette, R., Marre, O., Bertin, S., et al. (2021). Optogenetic therapy: high spatiotemporal resolution and pattern discrimination compatible with vision restoration in non-human primates. Commun. Biol. *4*, 125.
18. Gradinaru, V., Zhang, F., Ramakrishnan, C., Mattis, J., Prakash, R., Diester, I., Goshen, I., Thompson, K.R., and Deisseroth, K. (2010). Molecular and cellular approaches for diversifying and extending optogenetics. Cell *141*, 154–165.
19. Shevchenko, V., Mager, T., Kovalev, K., Polovinkin, V., Alekseev, A., Juettner, J., Chizhov, I., Bamann, C., Vavourakis, C., Ghai, R., et al. (2017). Inward H+ pump xenorhodopsin: Mechanism and alternative optogenetic approach. Sci. Adv. *3*, e1603187.
20. Dong, C., Filipeanu, C.M., Duvernay, M.T., and Wu, G. (2007). Regulation of G protein-coupled receptor export trafficking. Biochim. Biophys. Acta *1768*, 853–870.
21. Duvernay, M.T., Zhou, F., and Wu, G. (2004). A conserved motif for the transport of G protein-coupled receptors from the endoplasmic reticulum to the cell surface. J. Biol. Chem. *279*, 30741–30750.
22. Bali, B., Gruber-Dujardin, E., Kusch, K., Rankovic, V., and Moser, T. (2022). Analyzing efficacy, stability, and safety of AAV-mediated optogenetic hearing restoration in mice. Life Sci. Alliance *5*, e202101338.
23. Rozenberg, A., Oppermann, J., Wietek, J., Fernandez Lahore, R.G., Sandaa, R.A., Bratbak, G., Hegemann, P., and Béjà, O. (2020). Lateral gene transfer of anion-conducting channelrhodopsins between green algae and giant viruses. Curr. Biol. *30*, 4910–4920.e5.
24. Liberman, M.C. (1978). Auditory-nerve response from cats raised in a low-noise chamber. J. Acoust. Soc. Am. *63*, 442–455.
25. Zierhofer, C.M., Hochmair-Desoyer, I.J., and Hochmair, E.S. (1995). Electronic design of a cochlear implant for multichannel high-rate pulsatile stimulation strategies. IEEE Trans. Rehabil. Eng. *3*, 112–116.
26. Duarte, M.J., Kanumuri, V.V., Landegger, L.D., Tarabichi, O., Sinha, S., Meng, X., Hight, A.E., Kozin, E.D., Stankovic, K.M., Brown, M.C., and Lee, D.J. (2018). Ancestral adeno-associated virus vector delivery of opsins to spiral ganglion neurons: implications for optogenetic cochlear implants. Mol. Ther. *26*, 1931–1939.
27. Madisen, L., Mao, T., Koch, H., Zhuo, J.M., Berenyi, A., Fujisawa, S., Hsu, Y.W.A., Garcia, A.J., 3rd, Gu, X., Zanella, S., et al. (2012). A toolbox of Cre-dependent optogenetic transgenic mice for light-induced activation and silencing. Nat. Neurosci. *15*, 793–802.
28. Bedbrook, C.N., Rice, A.J., Yang, K.K., Ding, X., Chen, S., LeProust, E.M., Gradinaru, V., and Arnold, F.H. (2017). Structure-guided SCHEMA recombination generates diverse chimeric channelrhodopsins. Proc. Natl. Acad. Sci. USA *114*, E2624–E2633.
29. Klein, R.L., Dayton, R.D., Leidenheimer, N.J., Jansen, K., Golde, T.E., and Zweig, R.M. (2006). Efficient neuronal gene transfer with AAV8 leads to neurotoxic levels of tau or green fluorescent proteins. Mol. Ther. *13*, 517–527.

30. Liu, H.S., Jan, M.S., Chou, C.K., Chen, P.H., and Ke, N.J. (1999). Is green fluorescent protein toxic to the living cells? Biochem. Biophys. Res. Commun. *260*, 712–717.

31. Maimon, B.E., Diaz, M., Revol, E.C.M., Schneider, A.M., Leaker, B., Varela, C.E., Srinivasan, S., Weber, M.B., and Herr, H.M. (2018). Optogenetic peripheral nerve immunogenicity. Sci. Rep. *8*, 14076.

32. Lin, J.Y., Knutsen, P.M., Muller, A., Kleinfeld, D., and Tsien, R.Y. (2013). ReaChR: a red-shifted variant of channelrhodopsin enables deep transcranial optogenetic excitation. Nat. Neurosci. *16*, 1499–1508.

33. Huet, A.T., and Rankovic, V. (2021). Application of targeting-optimized chronos for stimulation of the auditory pathway. Methods Mol. Biol. *2191*, 261–285.